JOURNAL OF GEOPHYSICAL RESEARCH, VOL. 93, NO. A9, PAGES 9841–9853, SEPTEMBER 1, 1988

Geographic Distribution of Lightning-Induced Electron Precipitation Observed as VLF/LF Perturbation Events

U. S. INAN, T. G. WOLF, AND D. L. CARPENTER

Space, Telecommunications and Radioscience Laboratory, Stanford University, Stanford, California

Expected occurrence characteristics of lightning-induced electron precipitation (LEP) events at longitudes of the western (110° W) versus eastern (71° W) United States are considered from the point of view of available trapped particle flux at the edge of the loss cone. Considering published data on nighttime fluxes of > 68 keV electrons observed at $L \simeq 2.5$, and for "direct" precipitation into the northern hemisphere induced by northern hemisphere lightning, the occurrence rate and flux levels are expected to be a factor of 20-200 higher in the west than in the east, assuming no significant variation in lightning source activity with longitude. Again assuming lightning sources in the north, it is predicted that at 71° W, "mirrored" precipitation into the southern hemisphere would involve precipitation fluxes 30-300 times higher than "direct" precipitation into the northern hemisphere. However, at 110° W and again assuming lightning in the north, southern hemisphere precipitation would tend to be limited to that small fraction of particles that were initially scattered into the northern loss cone and that were then backscattered from the northern atmosphere so as to reach the south. Preliminary experimental investigation of these predictions is based on observations of lightning-associated perturbations of two geographically separate subionospheric VLF/LF signal paths, one (48.5 kHz) originating at Silver Creek, Nebraska, and observed at Stanford, California, and the other (28.5 kHz) originating at Aguadilla, Peurto Rico, and observed at Lake Mistissini, Quebec. The association of the characteristic VLF signal perturbations with lightning is generally evidenced by simultaneous (within ~ 1 s) observation of single or multiple radio atmospherics. In most cases, high-resolution measurements of event signatures reveal a ~0.5-1 s delay between the atmospheric and event onset, as well as an ~ 1-s onset duration, consistent with theoretical predictions of a test particle model of the gyroresonant whistler-particle interaction. The data, considered in the light of previous observations in the southern hemisphere, provide qualitative support for several of the predictions based on considerations of the trapped flux level near the loss cone, in particular the prediction of comparable rates in the north at 110° W and the south at 71° W, and the prediction of substantially larger rates in the south than in the north near 71° W.

1. INTRODUCTION

Transient perturbations in the amplitude and/or phase of subionospherically propagating VLF/LF signals, observed in association with magnetospheric whistlers and commonly referred to as Trimpi events, are increasingly being used to study the lightning/whistler-induced precipitation of energetic radiation belt particles. Figure 1 provides a simplified description of the phenomenology of a Trimpi event, during which whistler wave energy, propagating along a particular ducted magnetospheric path, gives rise to transient and localized precipitation regions at the ionospheric projections of a high-altitude whistler-particle interaction region and there to abrupt changes in the Earth-ionosphere mode structure for subionospherically propagating signals [*Helliwell et al.*, 1973; *Lohrey and Kaiser*, 1979; *Carpenter and LaBelle*, 1982; *Inan and Carpenter*, 1987, and references therein]. Direct satellite- and rocket-based measurements of lightning-induced electron precipitation (LEP) bursts have also been reported [*Rycroft*, 1973; *Voss et al.*, 1984; *Goldberg et al.*, 1986], and test particle simulation of whistler-particle gyroresonant interactions has been used to predict temporal signatures of events at different L shells [*Chang and Inan*, 1985]. Most previously reported events were believed to involve radiation belt electrons in the 40-300 keV energy range with the L shell range of $2 < L < 3$ being a prime region of occurrence [*Carpenter and Inan*, 1987; *Chang and Inan*, 1985]. More recent observations have shown that events also occur at $L < 1.8$ and may involve lightning-induced precipitation of >MeV electrons from the inner radiation belt [*Inan et al.*, 1988*a*].

These recent results have established LEP events as a frequently occurring phenomenon and have demonstrated the direct removal of trapped electrons from the radiation belts in individual events. However, the importance of LEP events in the overall loss rates of radiation belt electrons has yet to be addressed; for this purpose, knowledge of the geographic distribution of LEP event occurrence is required. For example, we need to know whether event occurrence rates are higher in the south or the north at the same longitude (i..e, the hemispherical distribution), or in the east or the west in the same hemisphere (the longitudinal distribution). The purpose of this paper is to address questions of this type.

Most reported observations of Trimpi events were based on data acquired in the Antarctic or in the northern hemisphere at longitudes of the eastern United States. Furthermore, Palmer Station, Antartica ($L \simeq 2.4$, 64° W), a site of many recently reported observations of Trimpi events, is situated in the region of the South Atlantic anomaly. With data from such a limited longitude range, it was not possible to determine to what degree the observed characteristics (such as the high occurrence rates at Palmer) were a consequence of the proximity of the South Atlantic magnetic anomaly and/or concentration of lightning and thunderstorm centers near the eastern seaboard.

Paper number 7A9346.
0148-0227/88/007A-9346$05.00

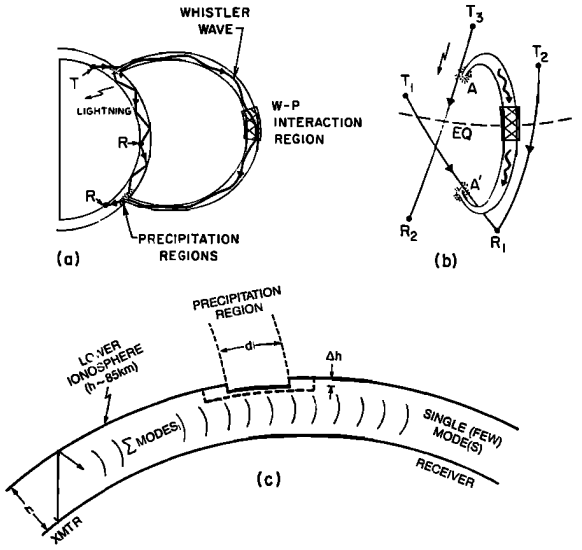

Fig. 1. Phenomenology of Trimpi events: (*a*) meridional plane projection of the field line of propagation showing a whistler wave launched by a lightning discharge propagating up the field line and interacting with energetic electrons in the vicinity of the equator; also shown is a subionospheric VLF/LF propagation path from a transmitter (T) to receiver(s) (R), (*b*) a three-dimensional sketch showing the spatial relationship of the whistler mode duct and subionospheric signal paths between transmitters (T_1, T_2, T_3) and receivers (R_1, R_2) that cross the precipitation regions (A, A'), and (*c*) a two-dimensional cross-sectional view of subionospheric propagation between a transmitter and receiver in the presence of a localized precipitation region, represented as a reduction Δh in the effective reflection height at the lower ionosphere over a region of length d.

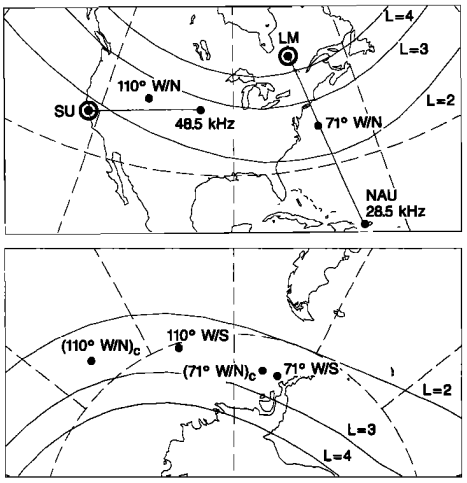

Fig. 2. Map showing the great circle propagation paths from the 48.5-kHz LF transmitter in Silver Creek, Nebraska, to Stanford (SU), California, and the 28.5-kHz NAU transmitter in Aguadilla, Puerto Rico, to Lake Mistissini (LM), Quebec. The loci of the footprint of the $L = 2, 3, 4$ field lines at 100 km altitude are indicated as continuous lines. Also shown for reference are the points (marked 71° W/N, 110° W/N, 71° W/S, and 110° W/S) at which four different $L \simeq 2.5$ field lines intersect the earth's surface. For two of the field lines, namely, 71° W/N and 110° W/N, the conjugate end points of the field lines are also indicated, marked as $(71°\ \mathrm{W/N})_c$ and $(110°\ \mathrm{W/N})_c$.

The geomagnetic latitude dependence of LEP event occurrence was addressed in previous work, and the L shell range of $2 < L < 3$ was identified as a prime region on the basis of theoretical modeling as well as observations [*Chang and Inan*, 1985; *Carpenter and Inan*, 1987]. In view of this L dependence of activity we shall examine the magnetospheric factors which influence the distribution of event occurrence in longitude and between hemispheres at $L \simeq 2.5$. To bring out longitude variations due to magnetospheric effects, the source lightning characteristics will be assumed to be uniform in longitude, although we recognize that in fact the lightning distribution and occurrence may well be determining factors in LEP event occurrence when time intervals as limited as a few months are considered. On the other hand, we note that on the basis of an annual average, the distribution of nighttime lightning over the continental United States can be quite uniform, especially between the eastern seaboard and the western edge of the Rocky mountains [*Orville and Henderson*, 1986].

To provide a quantitative basis for consideration of longitudinal and hemispherical dependences, we present in the following section profiles of the trapped energetic particle distribution in the vicinity of the loss cone, derived from published low-altitude satellite data [*Imhof et al.*, 1986] and from considerations of the Earth's magnetic field near the South Atlantic magnetic anomaly. This discussion formulates a number of predictions concerning event occurrence in longitude (east/west) and hemisphere (north/south) and is followed by a presentation of experimental results involving observations of Trimpi events on two subionospheric signal paths whose midpoints lie at $L \simeq 2.3$ at longitudes 110° W and 71° W, respectively (see Figure 2). Examples of high resolution temporal signatures are presented, in order to establish the association of the VLF perturbation events with lightning-generated radio atmospherics. The occurrence statistics of LEP event signatures on the two paths are described in a separate section; they provide qualitative support for several of the predictions about longitudinal and hemispherical differences.

2. Trapped Particle Distribution Near the Loss Cone; Implications for LEP Event Occurrence

Lightning-induced electron precipitation (LEP) events are inherently transient phenomena. Events generally consist of electron precipitation pulses of < 1 s duration; sometimes a sequence of pulses of decreasing intensity is observed and is interpreted as due to multiply reflected and backscattered electrons associated with the first pulse [*Voss et al.*, 1984; *Chang and Inan*, 1985]. The whistler wave traverses the entire field line in a time generally less than a few seconds, although wave echoing is also seen on occasion [*Doolittle and Carpenter*, 1983]. The available evidence suggests that an LEP burst consists of electrons that have been scattered into the bounce loss cone in a single encounter with a whistler wave packet. The transient nature of the lightning-excited whistler wave as well as the observed short duration of LEP pulses strongly indicate that a diffusion process, involving many bounces of the particles or of the wave, does not contribute significantly to the main precipitation pulse.

In such a circumstance, the absolute flux level of a given LEP pulse is most strongly dependent upon two parameters; (1) the magnetic field intensity of the whistler wave, and (2) the trapped electron flux level near the edge of the loss cone. The former is important, since it has been shown

that, especially at mid-to-low latitudes ($2 < L < 3$), most whistler-particle scattering involves primarily linear interactions, with the pitch angle scattering being proportional to the wave field intensity [*Chang and Inan*, 1985; *Inan*, 1987]. The trapped flux level at the loss cone edge is important, since for typical parameters of interest (e.g., wave magnetic field intensities of 5-50 pT and whistler frequencies of 0.5-6 kHz at $L \simeq 2.5$), pitch angle scattering of individual particles is estimated to be $0.1^\circ - 1^\circ$ [*Chang and Inan*, 1985]. Thus the shape or magnitude of the distribution at pitch angles more than a few degrees above the loss cone are not relevant. The dependence of the wave-induced precipitation flux on the near-loss-cone trapped particle distribution has been examined for the purpose of theoretical modeling of VLF transmitter-induced electron precipitation events observed on the S81-1 (SEEP) satellite [*Inan et al.*, 1985*b*].

The whistler wave intensity is determined by a number of highly variable factors, including the intensity of the lightning flash, the amount of VLF energy released during the flash, propagation of the wave energy within the earth-ionosphere waveguide and through the ionosphere and the magnetosphere, and possible amplification of the whistler as a result of wave-particle interactions. The following discussion is limited to the role of the near-loss-cone trapped particle distribution, which is a primary controlling factor for a given whistler wave spectrum.

To provide a basis for comparison within a limited longitude range, we consider the pitch angle variation of the trapped particle distribution at $L = 2.5$ and at two different longitudes, namely, 71° W and 110° W (close to the midpoint positions at $L \simeq 2.3$ on the two subionospheric paths shown in Figure 2). Based on data acquired on the low-altitude P78-1 satellite, *Imhof et al.* [1986] have published measured average fluxes of > 68 keV electrons locally mirroring at 600 km altitude in the latitude range of L=2.5-2.6 and in 20° geographic longitude intervals, both in the southern and northern hemispheres. Using these data and the first adiabatic invariant together with a model of the Earth's magnetic field [*Olson and Pfitzer*, 1974] equatorial pitch angle distributions were estimated on four different magnetic field lines that intersect 600 km altitude at $L = 2.5$ (1) at 71° W in the northern hemisphere, (2) at 71° W in the southern hemisphere, (3) at 110° W in the north, and (4) at 110° W in the south. The endpoints of these four field lines are shown in Figure 2, and the estimated pitch angle distributions are shown in Figure 3. Note, for example, that for the distribution for 71° W in the north (endpoint marked as 71° W/N), one of the two data points on the profile corresponds to the satellite measurement at 600 km altitude, 71° W, and at $L = 2.5$. The second data point corresponds to the satellite measurements in the southern hemisphere, again at $L = 2.5$ and at 600 km altitude, but at 77° W, which is the approximate geographic longitude of the magnetic conjugate of the point in the north. This point is marked at $(71^\circ\ \mathrm{W/N})_c$ in Figure 2. The profile defined by these two points is relevant to LEP events that would be observed in the northern hemisphere at 71° W and at $L \simeq 2.5$. The equatorial integral fluxes representing the satellite data as measured at 600 km altitude are shown as circled points in Figure 3; they define the slope of the pitch angle distribution above the loss cone.

At the longitudes of the South Atlantic anomaly, the equatorial loss cone angle corresponding to a local pitch angle of 90° at 100 km altitude in the southern hemisphere is considerably larger than that corresponding to the same altitude in the northern hemisphere. As a result of this separation, the slope of the pitch angle distribution near the loss cone is particularly well defined for the cases of 71° W, as seen in Figure 3. For the 110° W cases, the data points are close together in pitch angle and the inferred slope of the distribution is highly dependent on averaging and measurement uncertainties. For the purpose of the following discussion, we constructed the profiles for 110° W by assuming that the slope of the pitch angle is nearly constant with longitude and thus equal to that for 71° W. The profiles obtained in this manner agree reasonably well with the circled data points. The assumption of a pitch angle profile that is nearly independent with longitude is consistent with measurements made on the P78-1 satellite (W. L. Imhof, private communication, 1988).

For energy deposition in the ionosphere, the equatorial loss cone angles corresponding to a local pitch angle of 90° at 100 km altitude are important. These loss cone angles,

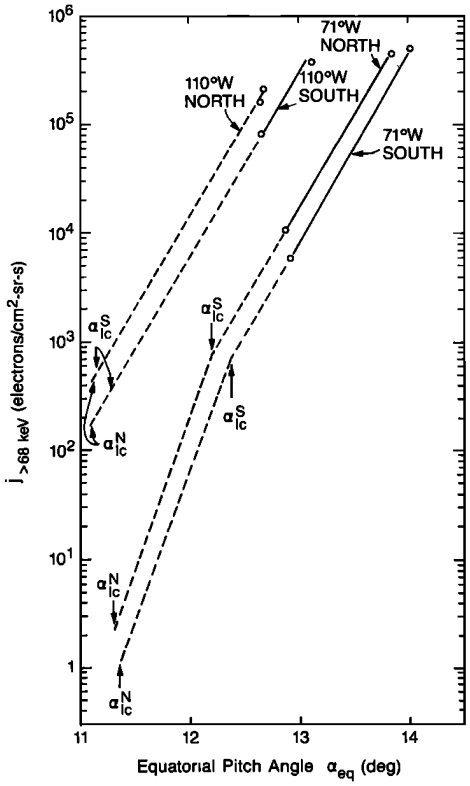

Fig. 3. Equatorial pitch angle distribution at $L = 2.5$ on four different magnetic field lines that intersect 600 km altitude (1) at 71° W geographic longitude and in the northern hemisphere, (2) at 71° W and in the south, (3) at 110° W geographic longitude and in the northern hemisphere, and (4) at 110° W and in the south. The data points are taken from P78-1 satellite measurements reported by (Imhof et al., 1986). The slope of the pitch angle distribution near the loss cone is assumed to be approximately constant with longitude over the range of 71° – 110° W [*W. L. Imhof*, private communication]. The equatorial loss cone angles ($\alpha_{lc}^{S,N}$) correspond to $\alpha = 90^\circ$ at 100 km altitude in the respective hemispheres and at the longitudes of 71° W and 110° W in the north and their respective conjugate regions (see Figure 2) in the south.

computed for the southern (α_{lc}^S) as well as northern (α_{lc}^N) hemisphere, are shown in Figure 3 for each of the four profiles.

Assuming that the shape of the pitch angle distribution near the loss cone is determined primarily by the interaction with the atmosphere [*Davidson and Walt*, 1977], the distribution for $\alpha_{eq} > \alpha_{lc}^S$ is taken to be an extension of the distribution represented by the 600 km points in Figure 3. For $\alpha_{eq} < \alpha_{lc}^S$ the distribution would be expected to decrease more rapidly with decreasing equatorial pitch angle, due to the loss of electrons during encounters with the southern hemisphere ionosphere. A further increase in slope would be expected for $\alpha_{eq} < \alpha_{lc}^N$, since electrons in this range would interact with the atmosphere in both hemispheres and thus would be subject to a higher percentage loss per bounce. No data exist that would allow accurate determination of the slope of the distributions for $\alpha_{lc}^N < \alpha_{eq} < \alpha_{lc}^S$; however, in a theoretical model study of transmitter-induced precipitation events, the best agreement with the satellite data on precipitating electrons was found using loss-cone distributions with a flux level at $\alpha_{eq} = \alpha_{lc}^N$ roughly an order of magnitude below that obtained from a simple extrapolation of the distribution for $\alpha_{eq} > \alpha_{lc}^S$ [*Inan et al.*, 1985]. On this basis we can construct the dashed line distributions of Figure 3, which then define the loss-cone distribution for $\alpha_{eq} > \alpha_{lc}^N$. Since the distribution between α_{lc}^N and α_{lc}^S is inferred on the basis of this indirect argument, we can only expect it to be accurate within an order of magnitude. Note that for 110° W, the difference between α_{lc}^N and α_{lc}^S is $< 0.1°$, which is negligible compared to individual particle scattering suffered during whistler-particle interactions or interactions with the atmosphere. Thus for practical purposes we consider $\alpha_{lc}^N \simeq \alpha_{lc}^S$, for 110° W.

The distributions of Figure 3 for 71° W longitude indicate that the flux level at $\alpha_{eq} = \alpha_{lc}^S$ on the 71° W/south profile is a factor of 30-300 larger than that at $\alpha_{eq} = \alpha_{lc}^N$ on the 71° W/north profile (The range 30-300 recognizes the uncertainty in the estimation of the distribution between α_{lc}^N and α_{lc}^S). This implies that for lightning in the northern hemisphere and for a whistler wave of given intensity, peak fluxes in "mirrored" precipitation events (south-going wave scatters north-going electrons that precipitate in the southern hemisphere after first mirroring in the north) [*Chang and Inan*, 1983] would be 30-300 times larger than those in "direct" precipitation events (south-going whistler scatters north going electrons that precipitate in the north). This conclusion is derived from the finding that whistler-induced fluxes that precipitate generally consist of electrons within $0.1° - 1°$ of the loss cone. Particles precipitating in the north (i..e, $\alpha_{eq} < \alpha_{lc}^N$), would have to originate at pitch angles just above $\alpha_{eq} = \alpha_{lc}^N$, and those that precipitate in the south at pitch angles just above $\alpha_{eq} = \alpha_{lc}^S$. The expectation of higher fluxes in mirrored precipitation events is consistent with studies that show high occurrence rates of VLF/LF events on subionospheric signal paths to Palmer and Siple, Antarctica, stations. These usually occur in time-correlation with whistlers originating in northern hemisphere lightning, and thus have been interpreted as mirrored precipitation [*Carpenter and LaBelle*, 1982; *Leyser et al.*, 1984; *Inan et al.*, 1985; *Inan and Carpenter*, 1986; 1987].

At 110° W, the difference between α_{lc}^S and α_{lc}^N is much smaller than at 71° W. With typical wave-induced pitch angle changes of 0.1°-1°, occurring during the first hop of the wave, and assuming only small effects due to additional hops, most precipitation can be expected to occur in the hemisphere of the lightning. In the typical case of northern lightning, southern hemisphere precipitation would tend to be limited to that small percentage of the particles that were initially scattered into the northern loss cone and that were then backscattered from the northern atmosphere so as to reach the south.

Comparing precipitation in the northern hemisphere at the two longitudes, the profiles of Figure 3 suggest that on the basis of the flux levels just above $\alpha_{eq} = \alpha_{lc}^N$ for the northern hemisphere profiles, we can expect 20-200 times larger precipitation fluxes at 110° W than at 71° W. For northern hemisphere lightning, direct precipitation in the northern hemisphere at 110° W longitude can be expected to involve occurrence rates and flux levels similar to those of mirrored precipitation in the southern hemisphere at 71° W, since the flux level for 110° W/north at α_{lc}^N is approximately equal to that at α_{lc}^S for 71° W/south. Comparing the two longitudes, the highest fluxes and/or occurrence rates would be expected to occur at 110° W for direct northern hemisphere precipitation and/or at 71° W for mirrored southern hemisphere precipitation.

In the rest of this paper we present initial results from an experiment aimed at investigating the geographic extent of Trimpi events. Simultaneous, high-resolution measurements of subionospheric VLF/LF signals were made at Stanford, California, and Lake Mistissini, Quebec. Figure 3 shows these two sites and the observation geometry for two particular subionospheric signal paths, the 48.5-kHz LF signal originating in Silver Creek, Nebraska, and observed at Stanford (SU), and the 28.5-kHz signal from the NAU transmitter in Aguadilla, Puerto Rico observed at Lake Mistissini (LM). Both of these signals are well positioned for detection of perturbations occurring in the L shell range of known high activity ($2 < L < 3$) [*Carpenter and Inan*, 1987], yet are geographically separate and are thus suitable for investigation of the questions raised above.

3. DESCRIPTION OF THE EXPERIMENTS

The VLF/LF data described here were acquired at Lake Mistissini (LM), Quebec (50° N, 74° W, $L \simeq 4.9$) and at Stanford (SU), California (37° N, 122° W, $L \simeq 1.8$) as part of a Stanford University program of subionospheric VLF/LF observations in the northern hemisphere. The geometry of the observations and sample subionospheric signal paths monitored are shown in Figure 4. The LM observation program was started in November 1986, and nearly continuous high-resolution recordings have been underway since March 1987. The Stanford observations have been ongoing on a more continuous basis, again since November 1986. Data are acquired during nighttime for ~12-14 hour periods (typically 2200-1200 UT at LM and 0100-1500 UT at SU). Amplitudes of the VLF/LF signals are measured using narrowband receivers with a 3-dB full bandwidth of ~ 300 Hz. The detected envelopes of the receiver outputs are sampled at a rate of 100 Hz. Averaging on site is used to obtain the lower sampling rates (typically 20 Hz or 50 Hz) at which the data are recorded on tape. Summary plots of the data from all channels are printed out at the end of each day; these

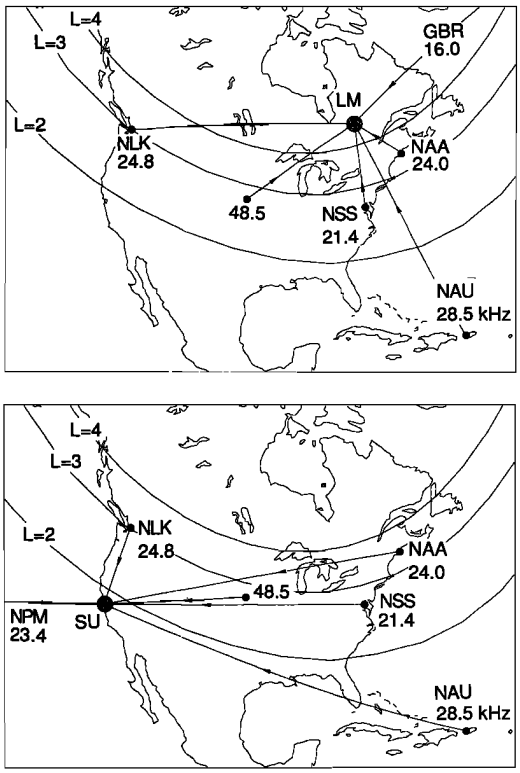

Fig. 4. Map showing the subionospheric VLF/LF paths generally observed at Stanford (SU), California, and at Lake Mistissini (LM), Quebec. The NPM transmitter is located in Lualualei, Hawaii, and the GBR transmitter is in Great Britain. The loci of the footprint of the $L = 2, 3, 4$ field lines at 100 km are also shown.

data were used for initial event identification as well as for the occurrence statistics reported in section 6 below.

At LM, broadband (0-30 kHz) VLF recordings are routinely made for 1 min out of every 5 or 15 min. These data are recorded on analog tape and are used for measurement of the frequency spectrum of spherics and whistlers (see Figure 12).

4. 48.5-kHz Signal Observed at Stanford

In this section we present examples of events observed at Stanford on the 48.5-kHz signal from the LF transmitter in Silver Creek, Nebraska, illustrating the association between the event temporal signatures and observed radio atmospherics. Figure 5 shows data from a 1-hour period on October 5, 1986, when a sequence of VLF perturbation events was observed. Data acquired for this case were first recorded in analog form without precise timing information. Thus the UT given on the upper right corner of Figure 5 is only accurate to within ± 1 min. The data were subsequently digitized at a rate of 50 Hz and are presented in this form. VLF events with the characteristic signature ($> 1\%$ change within < 1 s) were observed repeatedly during 0700-1230 UT. The data shown in Figure 5 represent a particularly active period during which 25 VLF events were observed, two of which involved very large ($> 30\%$) amplitude changes.

The lower panels in Figure 5 show the output of the 21.4 ± 0.15 kHz narrowband channel that is normally used to measure the 21.4-kHz signal from the NSS transmitter in Annapolis, Maryland (see Figure 4). During the period shown, this transmitter was not operating, thus facilitating use of this channel for detection of radio atmospherics. The nature of the noise background in this channel is highly impulsive, characteristic of VLF noise due to lightning. At an observation site such as Stanford, spherics from thunderstorm activity all around the world are received [*Helliwell*, 1965], and it is often difficult to identify spherics associated with particular events of interest. However, spherics associated with storms that are located nearby and/or are relatively isolated can be expected to be intense enough to stand out against a background of weaker impulses. In the case of the 48.5-kHz signal observed at Stanford, most observed perturbations are expected to be associated with lightning activity in the Rocky mountain region, relatively close (< 2000 km) to the receiver. For this reason and because of the relatively low level of thunderstorm activity near Stanford itself, spherics associated with events on the 48.5-kHz signal tend to be detectable, as illustrated below.

Examination of Figure 5 shows that each of the $> 1\%$ signal changes on the 48.5-kHz signal is time-correlated with a spheric, within the ~ 4-s resolution of the compressed scale used to show the data. (Note that although the background noise modulation on the signal is significantly greater than 1%, amplitude changes of 1% are nevertheless detectable as a level change, since the noise statistics are constant over short (~ 1 s) time scales.) There are many spherics in addition to those that are time-correlated with the LF events; however, most of the spherics that are time-correlated stand out in terms of their amplitudes. Higher resolution analysis of these events shows that these spherics are in fact within < 1 s of the LF event onsets, as discussed further below.

The two most prominent events from Figure 5 are displayed with higher time resolution in Figure 6, again with the signal output from the 21.4-kHz channel as a measure of spherics. A 10-s period approximately centered around the event onset is shown, with both the 48.5-kHz signal amplitude and the spheric channel output time-averaged over only 20 ms. The spherics preceding the event onsets are clearly seen with this resolution, both on the spheric channel and superimposed on the 48.5-kHz signal itself. The delay between the spheric and the event onset is in both cases ~ 0.5 s, and the duration of the event onset, or rise time (as measured between the 10% and 90% points) is also ~ 0.5 s. Both of these values are consistent with the predicted signatures of lightning-induced electron precipitation (LEP) events resulting from gyroresonant interactions in the magnetosphere between energetic (> 40 keV) electrons and whistler waves [*Chang and Inan*, 1985], thus providing support for the hypothesis that the observed subionospheric signal perturbations are ionospheric signatures of LEP events.

High-resolution analyses were conducted of all events observed during the 1-hour period displayed in Figure 5. In all, 25 events were identified as having transitions (amplitude changes) of $> 1\%$ in less than 2 s. A search was conducted for large spherics within 2 s of the onset of the transition; often more than one such spheric was found, and the most intense one among these was inferred to be the causative spheric. The delay times from spheric to event onset were measured with an accuracy of ± 0.2 s, and onset durations (rise times) from start to end of the transition were also

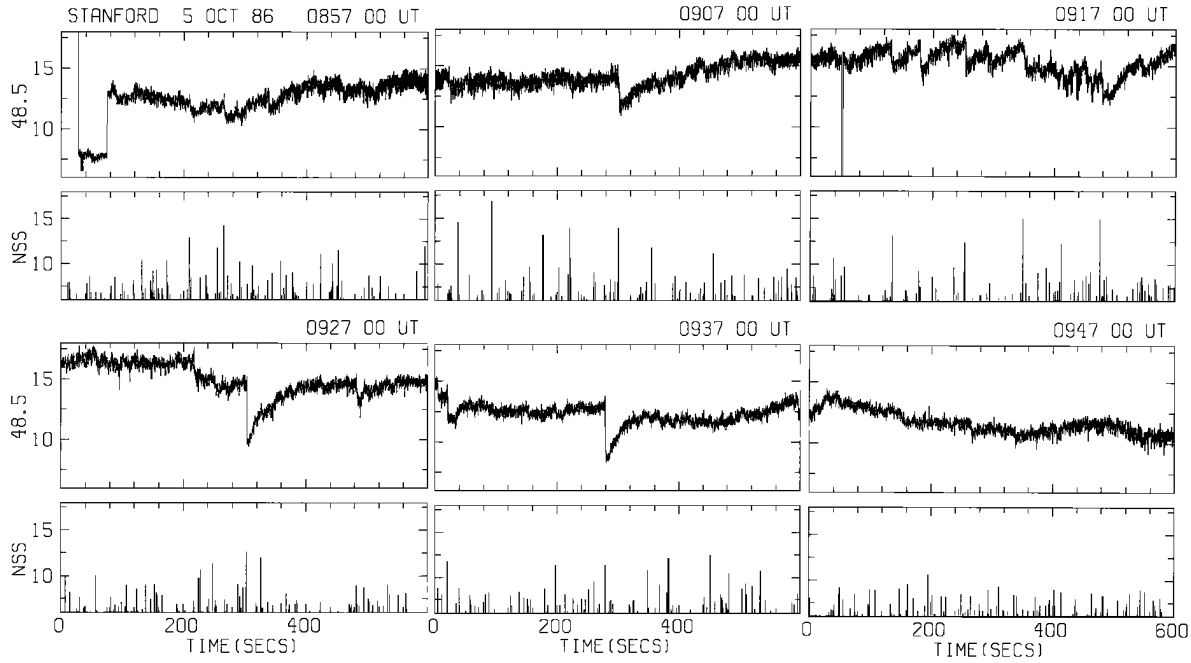

Fig. 5. A 1-hour sequence of perturbation events observed at Stanford on the 48.5-kHz signal. The top panels of each subframe show the intensity (A) of the 48.5-kHz signal in linear arbitrary units, with $A = 0$ representing the absence of signal, as measured within a bandwidth of $\sim$ 300 Hz and time averaged over 160 ms. The lower panels show the output of the 21.4±0.15 kHz channel, which is generally used to measure the 21.4-kHz NSS transmitter signal (see Figure 3) but is used here to detect the spheric activity, since NSS was not transmitting at this time. The data in the lower panels are time averaged over only 40 ms; the signal intensity (A) in the $\sim$ 300-Hz band is displayed in linear arbitrary units, with $A = 0$ representing the absence of signal. The data shown were originally acquired in analog form without the use of an absolute time reference; thus the start time of the 1 hour period, indicated as 0857 UT, is accurate to within ±1 min. For each 10-min subframe, the UT given in the upper right corner corresponds to $t = 0$ s as shown on the abcissa.

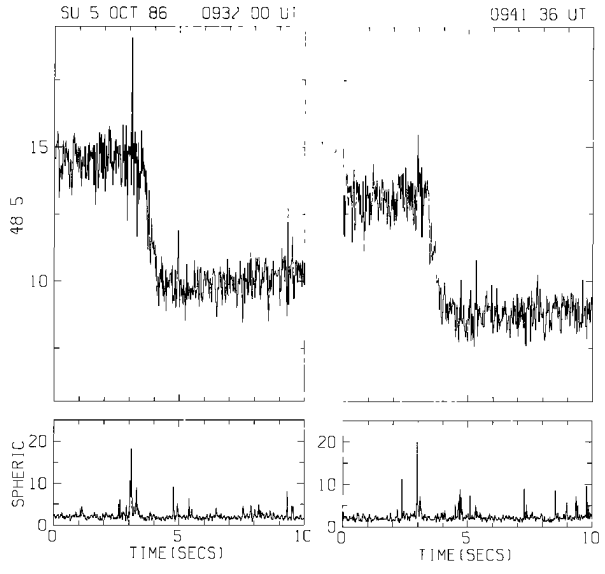

Fig. 6. High resolution displays of the two largest LF perturbation events shown in Figure 5. The upper panels show the intensity in a $\sim$ 300 Hz band centered around 48.5 kHz in the same format as Figure 4, except with time averaging over only 20 ms. The lower panels show the 21.4 kHZ channel (NSS) output, again averaged over 20 ms. As in Figure 5, the signal intensity in this channel is used as a measure of the spheric activity, since the NSS transmitter was not operating at the times shown. The causative spheric is seen both in the lower panels as well as in the upper panels, where the strong, impulsive spheric superimposed on the 48.5-kHz signal is clearly identifiable.

measured to within ±0.2 s. All events with rise times > 1 s were examined for the presence of additional spherics during the transition, possibly prolonging the onset duration. Finally, all events were examined to see whether the inferred causative spheric was the dominant one in the 20-s interval surrounding the event.

It was found that all but one of the 25 LF events had one or more well-defined spherics in the 1-s period preceding the onset. All events with rise times > 1 s had additional spherics occurring during the transition. In 13 of 25 events, the causative spheric (identified as the largest spheric within $\sim$ 2 s of the onset) was the dominant one visible in the surrounding 20-s interval. The average of the observed time delays was found to be $\sim$ 0.66 s, and the average rise time for all values of rise time < 1 s was found to be $\sim$ 0.47 s.

Another example of a 48.5-kHz signal perturbation observed at Stanford is illustrated in Figures 7 and 8. The 48.5 signal amplitude during a 400-s period on March 10, 1987, is shown in the top panel of Figure 7, together with the amplitude output of the 21.4-kHz (NSS) and 28.5-kHz (NAU) channels. Both of these transmitter signals were at a relatively low level, thus facilitating detection of atmospherics superimposed on the signals. The 48.5-kHz signal perturbation is time-correlated with an intense spheric observed on both the NSS and NAU channels. A small simultaneous signal amplitude change is also evident on the NSS signal, indicating that the perturbed ionospheric region(s) may have had a south-north extent large enough to ovelap both the 48.5-kHz SU and the NSS-SU paths (see Figure 4). Following the onset of the perturbations due to the spheric

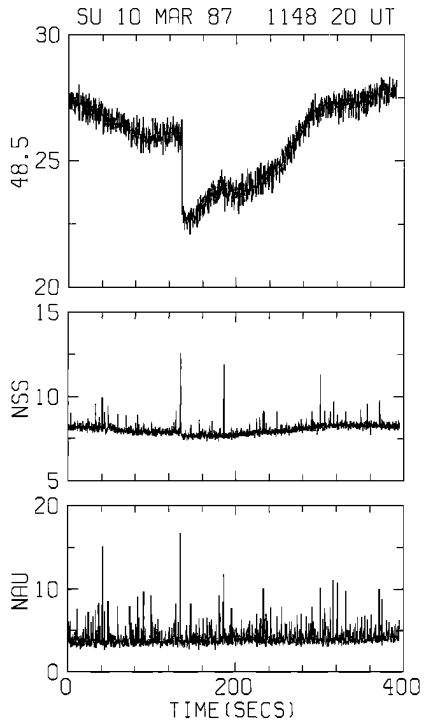

Fig. 7. An isolated perturbation event observed at Stanford on the 48.5-kHz signal. The top panel shows the intensity (A) of the signal with time averaging over 200 ms. The lower panels show channels used to detect the spheric activity, since their signal levels were rather low at the time of the observation. The data in the lower panels were also time averaged over 200 ms. A large spheric is visible in both of the lower panels at the onset time of the 48.5-kHz signal perturbation. A smaller perturbation (i.e., a level change) is also seen on the NSS signal, which arrives at the receiver from a direction similar to that of the 48.5-kHz signal (see Figure 4). The UT shown in the upper right corner is accurate to within ±10 ms.

at ~ 135 s in Figure 7, the recovery of the 48.5-kHz signal level to the preevent level appears to be interrupted at the time of a second spheric occurring at ~ 180 s. The event signature corresponding to the second spheric is unusual; there is no sudden signal level change, as in previously reported cases (see Figure 10) of Trimpi events in which a second event occurs before the recovery from the first is completed [*Inan and Carpenter*, 1986; *Inan et al.*, 1988*a*]. However, both the rate of recovery and the total recovery time appear to have changed, suggesting either that new ionization has been introduced or that the shape of the altitute profile of ionization have been altered. High-resolution analysis indicated that the interruption of the recovery occurred within ±25 ms (measurement resolution) of the time of the second spheric. The data was not sufficient to determine whether the spheric occurred before or after the interruption of the recovery. This apparent near simultaneous occurrence may simply be a coincidence, or it could represent direct coupling between cloud tops and the lower ionosphere as has been suggested on the basis of other data [*Armstrong*, 1983; 1987; *Inan et al.*, 1988*b*].

A high-resolution temporal signature of the onset of the event of Figure 7 is presented in Figure 8, together with the output of the NSS and NAU channels for spheric identification. The causative spheric is clearly visible on top of the 48.5-kHz signal itself as well as in the spheric channel. The delay between spheric and event onset for this case is ~ 0.8 s, and the onset duration (i.e., rise time) is ~ 1 s. The differences between these values and those measured in the case of Figure 6 can be attributed to differences in L shell, cold plasma density, trapped particle distribution and the whistler frequency spectrum. In view of these factors, the ~ 0.8-s delay and ~ 1-s rise time are considered to be within the range predicted by the whistler-particle gyroresonant interaction model [*Chang and Inan*, 1985].

Because of the well-defined characteristic signature of the lightning-associated VLF/LF perturbation events, it is possible to identify these events from visual inspection of low-time resolution summary plots, as mentioned in section 3. Such analysis is the basis of the occurrence statistics presented in section 6. High time resolution features of events, as well as their associations with spherics, cannot be identified from such summary data. Those features and associations are usually similar to those illustrated in Figures 6 and 8, but on occasion, events with either very small (< 50 ms) delays (i.e., "early") and/or very short rise times (< 50 ms) (i.e., "fast") have been observed, as previously reported [*Armstrong*, 1983; *Inan et al.*, 1988*b*]. Such early/fast Trimpi-like signatures are not consistent with an equato-

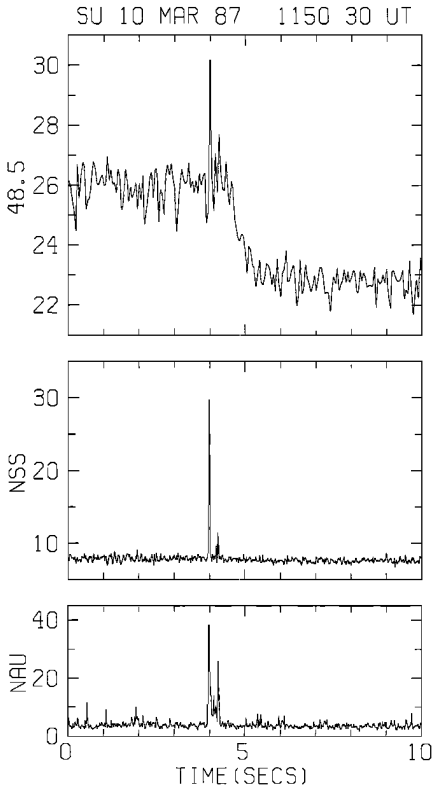

Fig. 8. High resolution display of the onset of the 48.5-kHz event shown in Figure 7. The format of this figure is the same as that of Figure 7, except that the signal intensity in the top panel is time averaged over only 50 ms and those in the lower two panels over only 20 ms. The causative spheric is clearly evident superimposed on the 48.5-kHz signal, as well as on the lower two panels. The event onset is delayed with respect to the spheric by ~ 800 ms. The duration of the event onset (i.e., rise time) is ~ 1 s. The UT shown in the upper right corner is accurate to within ±10 ms.

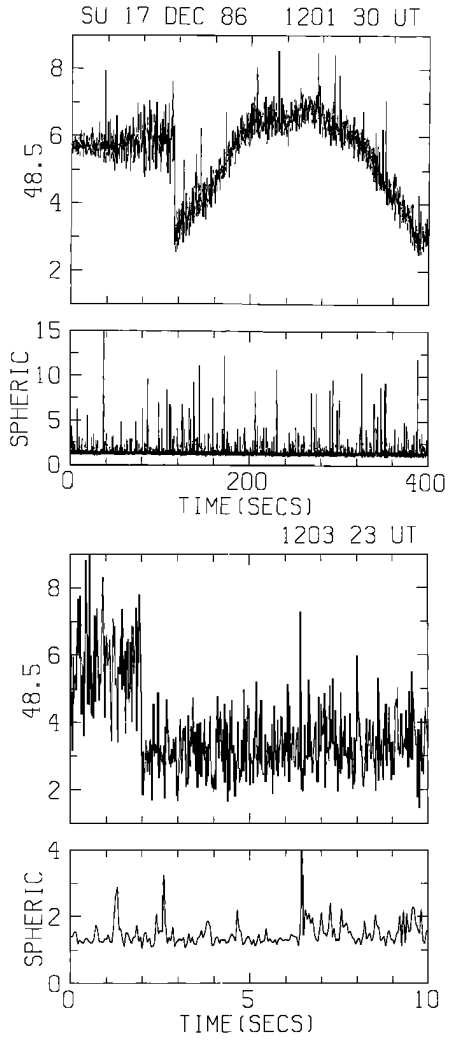

Fig. 9. An isolated 48.5-kHz perturbation event with an unusually "fast" rise time. The top two panels show a 400-s period displaying the event onset and the recovery signature. The 48.5-kHz signal shown in the uppermost panel is time averaged over 160 ms, whereas the output of the 37.2±0.15 kHz channel (used for spheric detection) is averaged over 50 ms. The format of the top two panels is otherwise similar to that of Figure 7. No causative spherics stand out as being associated with the event onset. The lower two panels show a 10-s period around the event onset. The 48.5-kHz signal intensity in the second panel from the bottom is time averaged over 20 ms, whereas the spheric channel output shown on the lowest panel is averaged over 50 ms. A possible causative spheric precedes the event onset by ~ 800 ms; however, other, stronger, spherics are observed before and after the event onset, and it is not possible to uniquely associate this particular spheric with the event onset.

rial gyroresonant model, and may be due to a more direct coupling mechanism between the lightning discharge and the ionospheric D region [*Armstrong*, 1987] or to whistler-particle resonant interactions occurring in the topside ionosphere [*Neubert et al.*, 1987]. "Fast," but not necessarily "early" events, with rise times of $\leq$ 50 ms can conceivably result from equatorial gyroresonant interactions, although they probably require a very specific set of conditions, such as a whistler wave in which the energy is confined to a narrow frequency range ($\leq$ 1 kHz) and/or whistler-particle interactions limited to a very narrow latitude range along the magnetic field line.

An example of a fast VLF perturbation event observed at Stanford on the 48.5-kHz signal is shown in Figure 9. On the 400-s scale of the top panel, the event is indistinguishable from others shown in Figures 5 and 7. However, the expanded records on the lower panels show that the duration of the event onset is extremely short, $\leq$ 100 ms. As in the previous cases shown above, the outputs of two other signal channels, here 37.2±0.15 and 24.0 ± 0.15 kHz (NAA), are

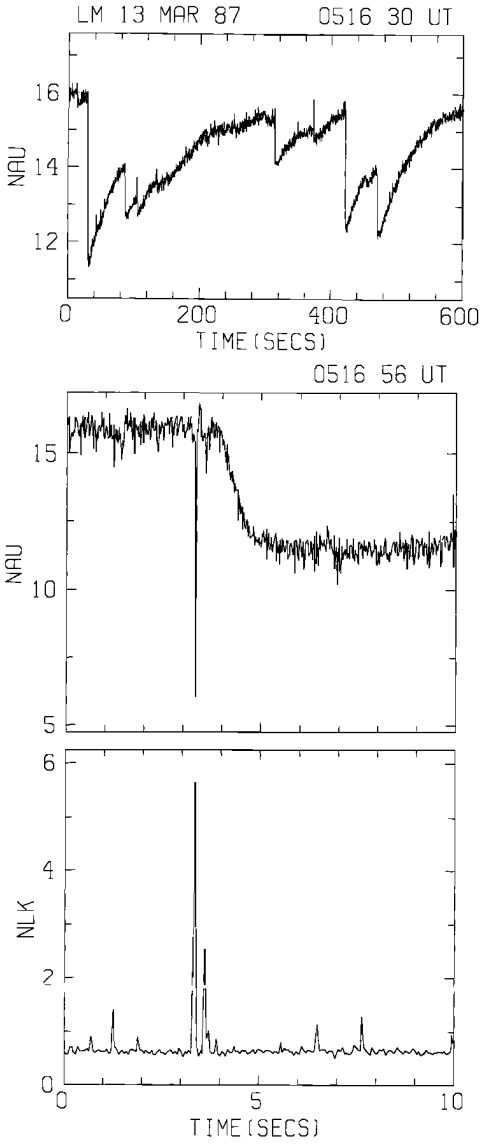

Fig. 10. Examples of perturbation events observed at LM on the 28.5-kHz NAU signal. (Detailed analysis of a 12-hour sequence of events observed on March 13, 1987, is reported in a separate paper [*Inan et al.*, 1988*a*]). The top panel shows a 10-min sequence in the same format as the upper panels of Figure 5. The signal intensity was time averaged over 320 ms. The middle panel shows high-resolution display, with 20 ms averaging, of the first event from the upper panel. The bottom panel shows intensity in the 24.8±0.15 kHz channel, time averaged over 50 ms. A pair of causative spherics are clearly evident in the NLK channel. The first, stronger, spheric momentarily saturates the 28.5-kHz channel since it is superimposed on the relatively strong transmitter signal.

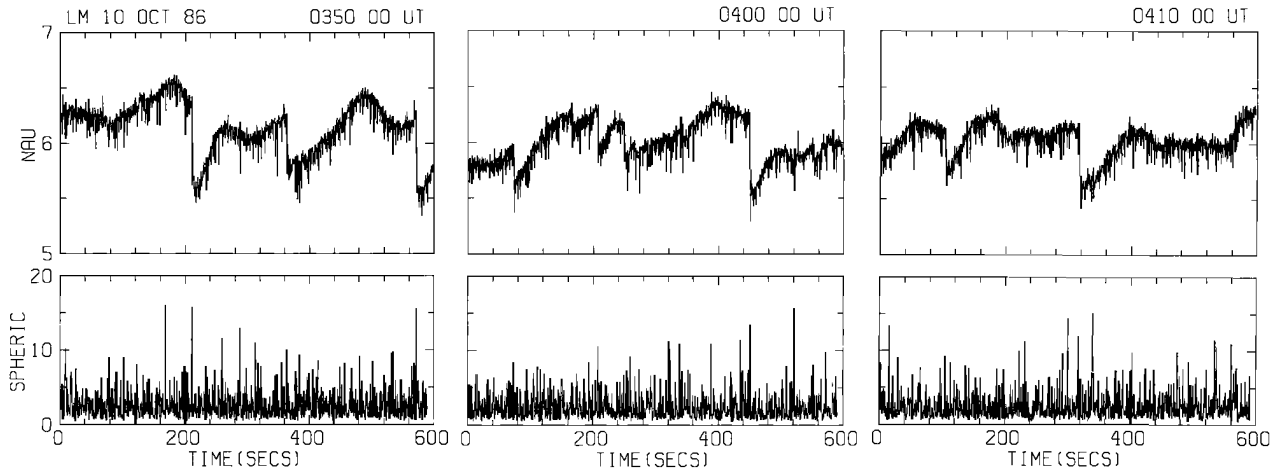

Fig. 11. A 30-min sequence of perturbation events observed at LM on the 28.5-kHz signal. The format of this figure is similar to that of Figure 5. The top panels show the 28.5-kHz signal time averaged over 320 ms, whereas the lower panels show the intensity in the 37.2±0.15 kHz channel, time averaged over 400 ms.

used for spheric identification. The former transmitter was not operating at the time, and the NAA signal level was low enough to allow easy detection of superimposed spherics. A relatively weak spheric apparently precedes the event onset by $\sim$ 800 ms, although there are other, stronger, spherics within a few seconds of the event onset. In this circumstance, and with only a single isolated event, it is not possible to uniquely identify the causative spheric. Thus we cannot determine whether this event is an "early" Trimpi event. However, the rise time of $\leq$ 100 ms is much shorter than typical values expected from whistler-particle gyroresonant interactions [*Chang and Inan*, 1985]. The lack of a strong observed spheric may be due to the fact that the causative lightning was very near the transmitter, and thus relatively far from Stanford. It is difficult to imagine the source of the perturbation as due to a signal level change at the transmitter itself, since the gradual recovery displayed is typical of Trimpi events. The recovery is believed to reflect the effective loss rate of excess electrons in the nighttime ionospheric D region [*Dingle and Carpenter*, 1981].

5. NAU (28.5-kHz) Signal Observed at Lake Mistissini

In this section we present examples of events observed at Lake Mistissini on the 28.5-kHz signal from the NAU transmitter in Aguadilla, Puerto Rico, in order to illustrate the association with radio atmospherics generated by lightning and the similarity of the event signatures to the 48.5 kHz events observed at Stanford.

The top panel of Figure 10 shows a 10-min sequence of events observed on March 13, 1987. In this sequence, the time-signature of an event that occurs before completion of the recovery from a previous one involves a sudden level change, as expected. On this day, a 12-hour sequence of unusually well defined events was observed in time correlation with cloud-to-ground lightning measured by the SUNY-Albany east coast lightning detection network [*Orville et al.*, 1987]. The VLF data and their association with lightning are reported in a separate paper [*Inan et al.*, 1988*b*]. In the present paper, we show the data of Figure 10 simply as a good example of VLF events observed at LM on the 28.5-kHz NAU signal.

The middle panel shows a 10-s segment around the onset of the first event from the top panel, while the bottom panel shows the output of the 24.8±0.15 kHz NLK transmitter channel used for spheric detection. The 28.5-kHz NAU receiver channel is momentarily saturated by the large causative spheric. The delay time between the spheric and event onset from Figure 10 is $\sim$ 0.7 s, while the rise time (onset duration) is $\sim$ 1 s.

Figure 11 shows a 30-min sequence of events observed on October 10, 1986. The top panels show the 28.5-kHz NAU signal amplitude and the lower panels spheric information in a 37.2±0.15 kHz channel. As in the case of Figure 5, examination shows that each of the > 1% signal changes on the NAU signal is time-correlated with a spheric, usually one of the stronger ones, within the $\sim$ 4-s resolution of the compressed scale used to show the data. On this day the stronger spheric activity tended to occur in the form of clusters of spherics, as shown in Figure 12, which compares the spheric activity as represented by the 37.2±0.15 kHz channel with the broadband 0-10 kHz spectrum. The latter was only recorded synoptically for 1 min out of every 15, and no VLF events were observed during the synoptic periods.

That the causative spherics associated with the VLF events also occurred in clusters is illustrated in Figure 13, where the top panel shows an expanded version of the first event from Figure 11. The middle panel shows the spheric channel output with only 50-ms averaging. Many spherics are evident, at levels comparable to or even higher than the spheric that is time-correlated with the event onset. The bottom panel shows the spheric channel output with 400-ms averaging. Most of the spherics are now averaged out, but the causative spheric stands out, since it consists of a cluster of spherics.

A high-resolution display of the same event is shown in Figure 14, with the spheric channel output on the bottom panel. The clustered nature of the causative lightning discharges is evident. The 28.5-kHz NAU channel is momentarily saturated by some of the larger spherics (see Figure 10), thus precluding accurate measurement of temporal features such as delay and onset duration (rise time). It is possible to conclude that the rise time is < 2 s, but the delay is not measurable, since the causative spheric cannot be uniquely identified. This result illustrates the limitations

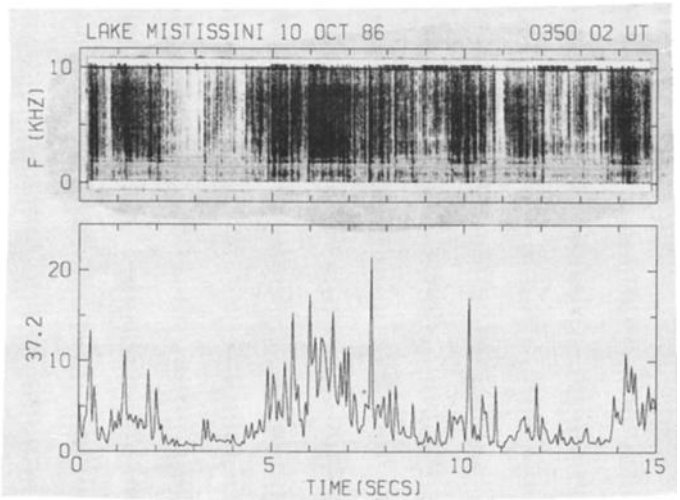

Fig. 12. Comparison of spheric activity as indicated by the signal intensity in the 37.2±0.15 channel with that measured with a broadband VLF receiver. Broadband recordings were only conducted synoptically during 1-min out of every 15, and no data were available during the perturbation events shown in Figure 11. The top panel shows the dynamic spectrum in the 0-10 kHz range, with darkness indicating the spectral intensity. The bottom panel is the output of the 37.2-kHz channel, displayed with 50-ms time averaging. The 37.2-kHz channel registers the clustered nature of the spheric occurrence on this day as well as single, intense spherics observed as sharp peaks.

of the subionospheric VLF technique in measuring temporal event features, under conditions in which the strong spherics occur in clusters of 1-3 s duration.

6. Occurrence Statistics

Statistics on the occurrence of Trimpi events on the 48.5-kHz signal path to Stanford and on the NAU path to LM

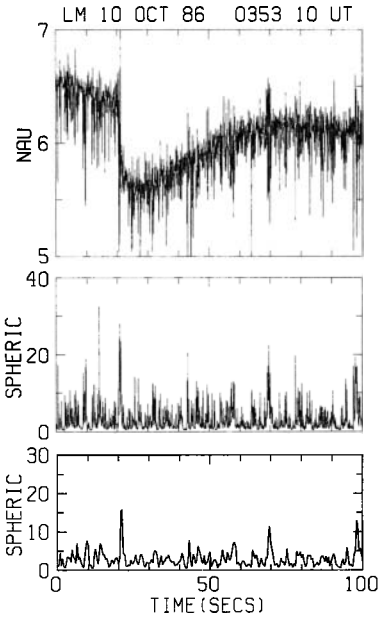

Fig. 13. Association of the 28.5-kHz perturbation events with clustered spherics. The top panel shows an expanded version of the first event from Figure 11, displaying the 28.5-kHz signal intensity with 40-ms time averaging, the middle panel the spheric channel (37.2±0.15 kHz) output with 50-ms averaging. The bottom panel shows the same with 400-ms averaging. While many spherics are seen in the middle panel, the causative spheric cluster (time correlated with the event onset) stands out after time averaging.

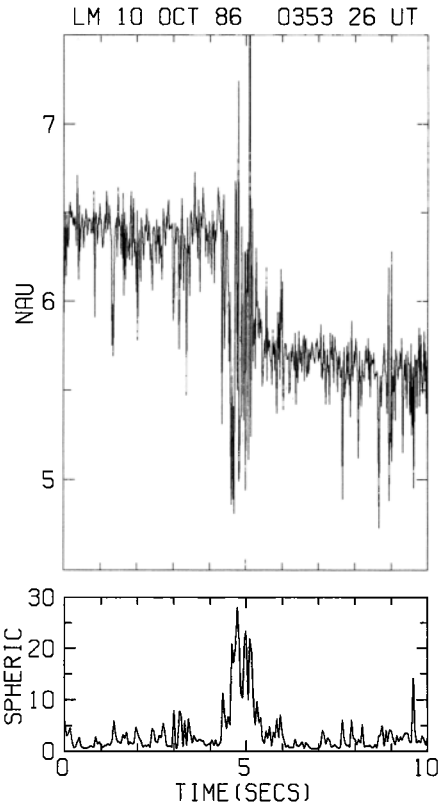

Fig. 14. High-resolution display of the perturbation event of Figure 13. The top panel shows the 28.5-kHz signal intensity with 20-ms time averaging, while the bottom panel shows the spheric channel output with 50-ms averaging. The temporal signature of the event onset (i.e., delay and rise time) are not measurable, since the spheric cluster, lasting for ~ 2 s, is superimposed on the 28.5-kHz transmitter signal. Some of the stronger spheric peaks momentarily saturate the receiver output (as was the case in Figure 10).

(Figure 2) were obtained by visual inspection of daily survey charts on which the amplitudes of the signals had been plotted after on site averaging (typically over 1-s). On these charts, the characteristic fast rise/slow decay signatures could be identified for amplitude changes of ~ 5% and greater. For the 48.5-kHz data at Stanford, analog charts were used until early November 1986. Figure 15 shows on a bar graph the number of hours within which one or more events were observed versus day of the year, from late September 1986 to early April 1987. A small solid circle indicates no activity, while a blank means that data were not available.

The statistical results from the survey charts were obtained entirely through inspection of those charts, and without regular recourse to high time resolution analysis. The survey charts were used as a basis for selecting individual events for detailed study, but there was no systematic use of the high time resolution data to check on errors in event recognition on the survey charts. Errors in the statistics are related to differences in the results obtained by different observers looking at the same data. These differences have been found to be greatest in the cases of observing days with one or two very small candidate events, and have not been found to affect the general features of the results such as those of Figure 15.

A remarkable feature of the data is the prolonged period

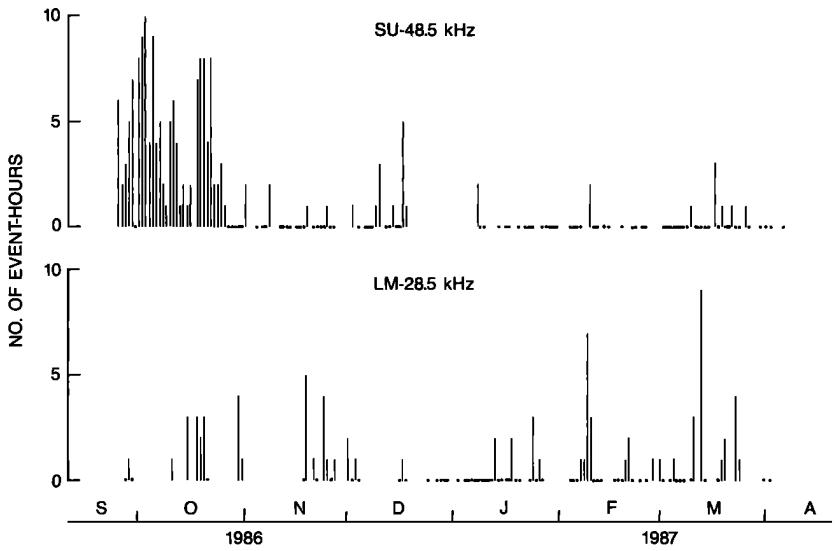

Fig. 15. Occurrence of perturbation events observed on the 48.5-kHz signal at Stanford and the 28.5-kHz signal at Lake Mistissini. For each observing day, the number of hours during which one or more VLF/LF perturbation events were detected is shown. Blanks indicate times when no recordings were made, whereas a dot indicates that data were acquired but no events were observed. Lake Mistissini, Quebec, is located at 50°N, 74°W and $L \simeq 4.9$, whereas Stanford is at 37°N, 122°W and $L \simeq 1.8$. See Figure 2 for an illustration of the subionospheric signal paths.

of high activity on the 48.5-kHz signal at Stanford during September-October 1986. In other periods the 48.5-kHz activity was sporadic, as was the activity on the NAU path. Days of event detection tended to occur in clusters, especially on the NAU-LM path. Unfortunately, observational coverage at LM was limited during the most active period on 48.5 kHz at Stanford.

Event occurrence rates are presented in Table 1 in terms of the number of hours during which the number of events detected (in the visual survey) fell within certain ranges. On the 48.5-kHz path to Stanford there were proportionately more hours with event rates > 5/hr, but most of the higher event rates occurred during the unusually active September-October 1986 period.

In comparing the results for the two paths in Figure 15, the days of occurrence from November through March are not obviously correlated, suggesting that they were individually dependent upon lightning source activity in well separated regions of propagation.

The occurrence data, in conjunction with previous reports from the southern hemisphere, provide a basis for qualitative testing of some of the predictions put forward in section 2 above. In terms of north/south hemisphere differences near 71° W, the activity in the south [*Carpenter and Inan*, 1987] appears to be substantially greater than that on the LM-NAU (28.5-kHz) path, in agreement with predictions. In terms of the north near 110° W and the south near 71° W, the 48.5-kHz Stanford activity in September/October 1986 was comparable to the high rates observed on signals recorded in previous campaigns at Palmer, Antarctica [*Carpenter and Inan*, 1987], again in agreement with prediction. There are indications that event activity west of Palmer and near $L = 2$ remains high over a distance of ~ 1500 km from the station, but a comparison of south versus north along the 110° W meridian is not yet possible, due to lack of data from the south.

7. Discussion and Concluding Remarks

The longitudinal and hemispherical distributions of lightning-induced electron precipitation (LEP) events are important in assessing the role of lightning and thunderstorms in the loss of radiation belt particles on a global scale. While the geographical distribution of thunderstorm and lightning activity is clearly important, longitudinal and hemispherical differences are also expected to occur because of the South Atlantic magnetic anomaly.

Lightning-induced electron precipitation events are inherently transient phenomena and all available evidence suggests that observed LEP bursts consist of electrons that have been scattered into the bounce loss cone in a single encounter with the whistler-wave packet. For this reason, a critical magnetospheric parameter that determines the absolute flux level for LEP pulses was recognized as the trapped electron flux near the edge of the loss cone. Using long-term-averaged polar satellite data on integral electron fluxes near the equatorial loss cone, we have estimated the near-loss-cone levels and pitch angle dependence of the integral flux at $L \sim 2.5$ at two longitudes west of the magnetic anomaly, 71° W and 110° W, and in both hemispheres. We have then examined the occurrence of perturbations on two longitudinally separated northern hemisphere VLF/LF signal paths as a qualitative test of the theoretical predictions.

In this first report we have illustrated characteristic signatures of the signal perturbations and in particular demonstrated how, through use of multiple signal channels, the radio atmospheric associated with the causative lightning can frequently be identified. Limitations on time resolution of features imposed by the clustering of atmospherics have also been indicated. In most cases, the highly time resolved signatures can be attributed to an equatorial gyroresonance scattering interaction. However, cases have been found of "fast" changes, involving transitions occurring within < 100

TABLE 1. Event Occurrence Rates at SU and LM

	Number of Event Hours at	
	SU	LM
Event Rate, number/hour		
1–5	121	67
6–10	26	9
11–15	6	2
16–20	6	2
21–25	3	0
26–30	2	0
31–35	2	0
36–40	4	0
46–50	1	0
Total	171*	80
Peak Amplitude		
< 10%	64	30
10–30%	74	40
> 30%	14	10
Total	152*	80

*Different because of saturation effects on amplitude.

ms as compared to the usual $\sim$ 0.5-1.0 s. Perturbation events with such fast transitions are similar to others reported by *Armstrong* [1987] and *Inan et al.* [1988*b*] suggest the possibility of some form of relatively direct coupling between the lightning discharges and the ionospheric D region.

The occurrence data on the two northern paths provide qualitative support for the theoretical predictions developed in section 2, in particular the prediction, at $L \simeq 2.5$, of comparable precipitation at 110° W in the north and 71° in the south, and the prediction of larger activity at 71° W in the south than in the north.

Since the theoretical predictions assume uniform lightning activity and also are based on long-term-averaged particle data, it is clear that in the VLF/LF signal studies, substantial coverage in time is needed in order to avoid variations in lightning activity. For example, part of the sharp drop-off in the SU 48.5-kHz activity after October 1986 may have been due to greater month-to-month variability in LEP-causing lightning activity than is typically the case for signal paths near 71° W in the south. On the other hand, both the problems of theoretical predictions and experimental investigation are simplified by the fact that in the longitude range ~60-120° W, most of the lightning affecting the region poleward of $L \sim 2$ occurs in the northern hemisphere.

Acknowledgments. We thank our colleagues at the STAR Laboratory for many useful discussions, notably R. A. Helliwell. We are grateful to J. P. Katsufrakis for his direction of the Stanford field programs, including the establishment of the new station at Lake Mistissini, Quebec, and his early recognition of the potential use of the NAU (28.5 kHz) and the 48.5 kHz transmitters for Trimpi studies. We thank D. Shafer and W. Burgess for their critical contributions to the acquisition and analysis of the Stanford and LM Trimpi data, and Scott Ferguson for his help in extracting the occurrence statistics from the summary plots. The manuscript was prepared by K. Fletcher. This research was supported by the National Science Foundation under grant ATM8415464 at Stanford University.

The editor thanks K. Bullough and another referee for their assistance in evaluating this paper.

REFERENCES

Armstrong, W. C., Recent advances from studies of the Trimpi effect, Antarct. J. 18, 281, 1983.

Armstrong, W. C., Lightning triggered from the Earth's magnetosphere as the source of synchronized whistlers, *Nature, 005*, 6121, 1987.

Carpenter, D. L., and U. S. Inan, Seasonal, latitudinal and diurnal distributions of whistler-induced particle precipitation events, *J. Geophys. Res., 92*, 3429, 1987.

Carpenter, D. L., and J. W. LaBelle, A study of whistlers correlated with bursts of electron precipitation near $L = 2$, *J. Geophys. Res., 87*, 4427, 1982.

Carpenter, D. L., U. S. Inan, M. L. Trimpi, R. A. Helliwell, and J. P. Katsufrakis, Perturbations of subionspheric LF and MF signals due to whistler-induced electron precipitation bursts, *J. Geophys. Res., 89*, 9857, 1984.

Chang, H. C., and U. S. Inan, A theoretical model study of observed correlations between whistler mode waves and energetic electron precipitation events in the magnetosphere, *J. Geophys. Res., 88*, 10,053, 1983.

Chang, H. C., and U. S. Inan, Lightning induced energetic electron precipitation from the magnetosphere, *J. Geophys. Res., 90*, 1531, 1985.

Davidson G., and M. Walt, Loss cone distributions of radiation belt electrons, *J. Geophys. Res., 82*, 48, 1977.

Dingle, B., and D. L. Carpenter, Electron precipitation induced by VLF noise bursts at the plasmapause and detected at conjugate ground stations, *J. Geophys. Res., 86*, 4597, 1981.

Doolittle, J. H., and D. L. Carpenter, Photometric evidence of electron precipitation induced by first hop whistlers, *Geophys. Res. Lett., 10*, 611, 1983.

Goldberg, R. J., J. R. Barcus, L. C. Hale, and S. A. Curtis, Direct observation of magnetospheric electron precipitation stimulated by lightning, *J. Atmos. Terr. Phys., 48*, 293, 1986.

Helliwell, R. A., *Whistlers and Related Ionospheric Phenomena*, Stanford University Press, Stanford, Calif., 1965.

Helliwell, R. A., J. P. Katsufrakis, and M. L. Trimpi, Whistler-induced amplitude perturbation in VLF propagation, *J. Geophys. Res., 78*, 4679, 1973.

Imhof, W. L., H. D. Voss, M. Walt, E. E. Gaines, J. Mobilia, D. W. Datlowe, and J. B. Reagan, Slot region electron precipitation by lightning, VLF chorus, and plasmaspheric hiss, *J. Geophys. Res., 91*, 8883, 1986.

Inan, U. S., Gyroresonant pitch angle scattering by coherent and incoherent whistler mode waves in the magnetosphere, *J. Geophys. Res., 92*, 127, 1987.

Inan, U. S., and D. L. Carpenter, On the correlation of whistlers and associated subionospheric VLF/LF perturbations, *J. Geophys. Res., 91*, 3106, 1986.

Inan, U. S., and D. L. Carpenter, Lightning-induced electron precipitation events observed at $L \simeq 2.4$ as phase and amplitude perturbations on subionospheric VLF signals, *J. Geophys. Res., 92*, 3293, 1987.

Inan, U. S., D. L. Carpenter, R. A. Helliwell, and J. P. Katsufrakis, Subionospheric VLF/LF phase perturbations produced by lightning-whistler induced particle precipitation, *J. Geophys. Res., 90*, 7457, 1985*a*.

Inan, U. S., H. C. Chang, R. A. Helliwell, W. L. Imhof, J. R. Reagan, and M. Walt, Precipitation of radiation belt electrons by man-made waves: A comparison between theory and measurement, *J. Geophys. Res., 90*, 359, 1985*b*.

Inan, U. S., W. C. Burgess, T. G. Wolf, D. C. Shafer, and R. E. Orville, Lightning-induced precipitation of MeV electrons from the inner radiation belt, *Geophys. Res. Lett.*, 1988*a*.

Inan, U. S., D. C. Shafer, W. Y. Yip, and R. E. Orville, Subionospheric VLF perturbations observed in association with lightning, (*J. Geophys. Res.*, in press), 1988*b*.

Leyser, T., U. S. Inan, D. L. Carpenter, and M. L. Trimpi, Diurnal variation of burst precipitation effects on subionospheric VLF/LF signal propagation near $L = 2$, *J. Geophys. Res., 89*, 9139, 1984.

Lohrey, B., and A. B. Kaiser, Whistler-induced anomalies in VLF propagation, *J. Geophys. Res., 84*, 5121, 1979.

Neubert, T., T. F. Bell, and L. R. O. Storey, Resonance between coherent whistler mode waves and electrons in the topside ionosphere, *J. Geophys. Res., 92*, 255, 1987.

Olson, W. P., and K. A. Pfitzer, A quantitative model of the magnetospheric magnetic field, *J. Geophys. Res., 79*, 3739, 1974.

Orville, R. E., and R. W. Henderson, Global distribution of midnight lightning: September 1977 to August 1978, *Mon. Weather Rev., 114*, 2640, 1986.

Orville, R. E., R. A. Weisman, R. B. Pyle, R. W. Henderson, and R. E. Orville, Jr., Cloud-to-ground lightning flash characteristics from June 1984 thrugh May 1985, *J. Geophys. Res., 92*, 5640, 1987.

Rycroft, M. J., Enhanced energetic electron intensities at 100 km altitude and a whistler propagating through the plasmasphere, *Planet. Space Sci., 21*, 239, 1973.

Voss, H. D., W. L. Imhof, J. Mobilia, E. E. Gaines, M. Walt U. S. Inan, R. A. Helliwell, D. L. Carpenter, J. P. Katsufrakis, and H. C. Chang, Lightning induced electron precipitation, *Nature, 312*, 740, 1984.

D. L. Carpenter, U. S. Inan, and T. G. Wolf, Space, Telecommunications and Radioscience Laboratory, Stanford University, Deptartment of Electrical Engineering, Durand 324, Stanford, CA 94305.

(Received October 13, 1987;
revised March 7, 1988;
accepted March 9, 1988.)